Carbohydrate Polymers 225 (2019) 115189

Contents lists available at ScienceDirect

Carbohydrate Polymers

journal homepage: www.elsevier.com/locate/carbpol

Characterization of nanocellulose and activated carbon nanocomposite films' biosensing properties for smart packaging

Abdus Sobhan, Kasiviswanathan Muthukumarappan, Zhisheng Cen, Lin Wei*

Agricultural & Biosystems Engineering Department, South Dakota State University, 1400 North Campus Drive, Brookings, SD 57007, United States

ARTICLE INFO

Keywords:
Activated carbon
Nanocellulose
Nanocomposite
Biosensor
Smart packaging

ABSTRACT

The goal of this research is to develop a functional nanocellulose and activated carbon (NAC) film and characterize its biosensing properties for smart packaging applications. The NAC film was prepared from activated carbon powder and nanocellulose gel using the casting method. The nanocellulose contents in the films were varied from 15% to 50% (w/w). Physicochemical properties of the produced films such as electrical conductivity, water absorption capacity, solubility in water and mechanical properties were measured. The electrical conductivity of the NAC film decreased when nanocellulose content increased. The tensile strength (TS), strain and Young's modulus of films increased significantly from 0.03 to 4.78 MPa, 0.13 to 1.94% and 97.64 to 247.3 MPa, respectively, when the nanocellulose contents increased. Thermal stability was also determined using thermal gravimetric analysis (TGA) and differential scanning calorimetry (DSC). The results showed that thermal decomposition was occurred in a temperature range of 300–400 °C.

1. Introduction

Food scientists have become interested in electrochemical biosensor research because its potential for determining the quality of food more easily than conventional methods (Sobhan, Lee, Park, & Oh, 2019). Although many studies have been reported on the concept of biosensing for smart food packaging (Pacquit et al., 2006; Sozer & Kokini, 2009), biosensor-based packaging for food integrity and quality is not yet common. Indirect indigenization of biosensors in food packages is not suitable due to their poor selectivity, sensitivity and accuracy (Hayat et al., 2016). In addition, the structure of tiny biosensors for packaging is difficult due to their low signal properties (Biji, Ravishankar, Mohan, & Srinivasa Gopal, 2015). To overcome these limitations, direct electron transfer is preferred over package components, which ensures low cost, fast response and high sensitivity (Scognamiglio, 2013). In direct electrochemistry, the most commonly used ingredients are carbon (Jian, Ju, Hu, Deng, & Lei, 2009), gold (Sheng, Luo, Li, & Zheng, 2009), silver (Liu & Hu, 2009) and metal oxides (Najafi, Khalilzadeh, & Karimi-Maleh, 2014). They are used to promote improved electron transfer rates. Among these electro-promoters, carbon is a suitable and widely used material for electrocatalysis and electroanalysis (Sheng, Gao, Sun, & Gao, 2014). It has different forms, including graphene, carbon nanotube (single or multi-walled) and activated carbon (Mani, Devadas, & Chen, 2013).

Activated carbon (AC) was chosen for this study because it has recently attracted widespread attention because of its desirable physico- and electro-chemical properties, such as uniform porosity, large surface area, low toxicity, good electrical conductivity, and surface functionality (Sevilla, Yu, Zhao, Ania, & Titiricic, 2014; Sevilla-Solís & Fuertes-Arias, 2014). It has a mesoporous structure, which can absorb the gas or liquid molecules quickly because of its well-ordered pore structure, narrow pore size distribution and high specific surface area (Tasviri, Rafiee-Pour, Ghourchian, & Gholami, 2011). In addition, the adsorption properties of AC have been studied for their use in biosensors (Kim, Cho, Bae, & Lee, 2014). These unique properties of AC make an ideal support for the preparation of electrode materials in multiple applications, such as supercapacitors, batteries (Sevilla-Solís & Fuertes-Arias, 2014), catalysis and bioanalysis (Veerakumar et al., 2014). In the present study, nanocellulose was loaded with the AC in order to achieve a carbon film format that can work as conductive materials.

Cellulosic nanofibers (CNF) (4–25 nm diameter) have gained attention as reinforcement materials (Morán, Vázquez, & Cyras, 2013). They have unique and attractive features, including biodegradability, low expense, good chemical stability, low density and high aspect ratio (Gupta & Tripathi, 2011; Vigneshwaran, Mhaske, Savadekar, Karande, & Bharimalla, 2012). The alignment and orientation of CNF with polymer matrixes reforms ordered structures, making them good candidates for the design of sensing and biosensing film (Qiu, Zhang, &

* Corresponding author.
E-mail address: Lin.Wei@sdstate.edu (L. Wei).

https://doi.org/10.1016/j.carbpol.2019.115189
Received 8 May 2019; Received in revised form 24 July 2019; Accepted 9 August 2019
Available online 12 August 2019
0144-8617/

Zhao, 2011). Unfortunately, CNF materials are dielectric; however, the electrical conductivity of CNF can be improved by adding carbon materials like AC for uses in biosensing devices (Hayat et al., 2016).

Incorporation of CNF into the nanocomposite membrane is reported to exhibit electrical, mechanical and barrier properties, hence it garners significant scientific attention (Niazi, Jahan, Berg, & Gregersen, 2017). The surface charge of CNF is controlled by different chemical treatments, such as partial carboxymethylation and phosphorylation (Niazi et al., 2017). Nanocellulose modified with carbon materials (a single walled-carbon nanotube) is also reported as an efficient catalyst for electrochemical oxidation, which leads to remarkable electrochemical characteristics (Ortolani et al., 2019). In this study, a NAC film that combines the advantages of nanocomposites prepared with AC and CNF was fabricated to form mechanical, thermal and electrochemical sensing film for smart food packaging. It is expected to afford excellent adsorptive capacity, catalytic and conductive properties and offer potential use in smart food packaging. There are different kinds of the film have been made for the food packaging such as pectin and nano-cellulose film (Chaichi, Hashemi, Badii, & Mohammadi, 2017), starch film reinforced by laver (Chen et al., 2019), chitosan film (Remedio, dos Santos, Maciel, Yoshida, & de Carvalho, 2019); gelatin film (Jamróz et al., 2018); poly-lactic acid film (Cao et al., 2019) and so on. However, all of these films have poor mechanical characteristics and even they are not suitable for the use of electrical conductivity. Furthermore, although some films produced by conductive polymers, such as polypyrrole and polyaniline polymer, are reported in the literature for smart packaging (Jafari & Amini, 2019; Mohebi & Marquez, 2015), these films exhibit poor mechanical and thermal properties, consume the high cost of raw materials and its electrical current sensitivity fluctuates over the time (Liu, Sui, & Bhattacharyya, 2014). Depending on these features, the NAC film has been considered as an alternative to being potential for smart packaging, although the NAC film is still under developing. To the best of our knowledge, there is no similar research or NAC film used for smart food packaging was reported. The current study focuses on the NAC film preparation by combing AC and CNF and an analysis of their effects within various mechanical, physical and thermal conditions. The main goal of this research is to integrate the biosensor concept into smart food packaging. Therefore, the objectives of this study are to 1) prepare NAC films with various CNF and AC contents; and 2) observe the electrochemical, thermal and mechanical properties of CNF and AC film.

2. Materials and methods

2.1. Materials

The activated carbon (Norit® GAC 1240 Plus) was procured from Cabot Corporation (Georgia, USA). The purity of AC was greater than 98%. The aqueous gel of CNF (5–20 nm, crystalline index: > 87%, purity of 3%) was purchased from the Process Development Center at University of Maine (Orono, ME, USA). A 10% (v/v) phosphate buffer saline (PBS, 0.1 M, pH 7.4, 0.8% NaCl) was procured from Thermo Fisher Scientific and prepared by mixing with purified water. Potassium hexacyanoferrate $[K_2Fe(CN)_6]^{-3}$ was purchased Sigma Aldrich (St. Louis, MO, USA). The potassium chloride (KCl, purity ≥ 99.0%) used for our solution was bought from Sigma Aldrich (St. Louis, MO, USA). Throughout the experiments, triple distilled water was used.

2.2. Preparation of NAC films

To synthesize NAC films, the first step is to prepare CNF suspensions. 2.5 g of CNF aqueous gel was put into 30 mL of deionized water and then gently stirred at about 50 °C for 30 min to create a CNF suspension. Subsequently, based on calculation, different amounts of AC powder were individually added to the prepared CNF suspensions to get NAC mixtures with AC contents of 85%, 70% and 50% of dry weight, corresponding to CNF contents of 15%, 30% and 50% of dry weight. After that, the solution of NAC mixture was homogenized for 15 min to get a new NAC suspension using a hand-held homogenizer (PRO scientific, USA). After homogenization, 30 mL of each NAC suspension was poured into a petri dish for casting a NAC film. As different NAC suspensions were poured into petri dishes, they were dried to form NAC films in an oven at 60 °C for 12 h. The dried films were peeled from the petri dishes and then conditioned in a container at 50–60% relative humidity (RH) and room temperature for 2 days prior to any analysis or characterization. All different types of NAC films were prepared in triplicate for characterization. The final dried films were named according to the CNF contents and are termed 15%, 30% and 50% NAC films in this study. Thickness of the film was measured using a hand-held micrometer (Esslinger, MN, USA).

2.3. Characterization methods

2.3.1. Electrochemical properties

The NAC films were characterized electrically using linear sweep voltammetry (LSV), cyclic voltammetry (CV), differential pulse voltammetry (DPV) and electrochemical spectroscopy (EIS). For LSV measurement, a two electrode system was set up, where one of the multiple-input electrodes was considered as a working electrode and a common ground was used the counter electrode. The reference electrode and counter electrode from the instrument were linked to each other. To measure the resistances of NAC film, a 2-pair distance with 6 mm gaps was chosen as the base sensing platform (Sobhan, Oh, Park, Kim et al., 2018; Sobhan, Oh, Park, & Lee, 2018). A change in resistance was confirmed throughout the electrical responses inspected in NAC film. In this study, LSV measurements were done with a potentiostat device for each repetition (DY2013, Digi-Ivy, Inc., Austin, USA). The slope of the current/voltage curve obtained from 0.0 to 0.1 V for each measurement was calculated using linear regression analysis. Afterward, the resistance (Rs) was calculated from the inverse of current/voltage value (Sobhan, Oh, Park, & Lee, 2018). In this case, the experimental data from LSV are described as means and the standard deviations were calculated depending on the number of repeated tests.

CV and DPV measurements were performed to characterize the stepwise modification of the electrode surface. For these test, a gold working electrode (2 mm diameter), platinum wire as a counter electrode and Ag/AgCl (3.0 mol L^{-1} KCl) as a reference electrode, which were immersed in PBS buffer (pH 7.4) containing 2.5 mmol L^{-1} $[Fe(CN)_6]^{3-}$ and 0.1 mol L-1 KCl during the test (Sobhan, Oh, Park, & Lee, 2018; Sobhan, Oh, Park, Kim et al., 2018). 15%, 30% and 50% NAC were sequentially dropped onto the working electrode and the signals of CV and DPV were collected. The scan rate for CV and DPV was 100 mVs -1, while the potential ranged from $+0.6$ to -0.2 V. EIS technique was performed to compare the impedance properties of NAC films. The frequency range for EIS fluctuated between 0.1 and 10^6 Hz at an amplitude of 0.01 V using EC-lab software (Bio-Logic Science Instruments). All the experiments were completed at room temperature (20 ± 2 °C).

2.3.2. Thermal stability

Thermal properties of the NAC films were analyzed using a differential scanning calorimeter (DSC) (DSC-Q2000, TA Instruments, USA) and thermogravimetric analyzer (TGA) (Q5000 SA, TA Instruments, USA). Sample preparation for TGA and DSC was performed by following the procedure described previously with one minor modification (Farrag et al., 2018). 3 mg of each 15%, 30%, and 50% NAC film sample were directly placed into a hermetically sealed pan using a Tzero hermetic lid. Afterwards, the specimens were heated under a nitrogen atmosphere in the range of 20 – 400 °C with a heating rate of 10 °C/min and a gas flow rate of 20 ml/min. The reference was an empty aluminum pan.

2.3.3. Mechanical properties

The mechanical properties of NAC films were evaluated according with ASTM D882 (Sadegh-Hassani & Mohammadi-Nafchi, 2014). Prior to the test, the film strips were cut uniformly to 50 mm long and 20 mm wide. Afterwards, the strips were conditioned in a desiccator for 24 h at 25 °C at 50% relative humidity. A texture analyzer (Texture Technologies Corp., Scarsdale, NY, USA), equipped with Texture Exponent 32 software, was used to measure tensile force and deformation. The initial grip spacing and cross-head speed were set at 100 mm and 0.5 mm/s, respectively. Tensile strength, strain and Young's modulus of the films were calculated from the force and deformation data recorded by the software. Three replications of the NAC film were evaluated for each measurement. Tensile strength (TS), strain and Young's modulus were calculated using the following equation:

$$\mathrm{TS} = \frac{\text{Maximum applied force}}{\text{Film thickness} \times \text{Film width}} \quad (1)$$

$$\text{Strain} = \frac{\text{Elongation}}{\text{Original length of film}} \quad (2)$$

$$\text{Young's modulus} = \frac{\mathrm{TS}}{\text{Strain}} \quad (3)$$

2.3.4. Solubility in water

Solubility of the NAC film in water is defined as the dispersing rate of the film particles per weight of the NAC film into the water. It was determined by following the studies previously described with minor modification (Morán et al., 2013). To determine the water solubility of the films, they were cut into rectangular pieces (40 × 30 mm ≈ 200 mg) and stored in a desiccator with desiccant (P_2O_5) to keep RH ≤ 10% for 2 days. The initial weight of each film strip was recorded and then placed into beakers with 100 mL deionized water (18 MΩ). Afterwards, films were agitated with a constant stirring rate (300 rpm) for 1 h at room temperature. After stirring, the remaining pieces of the film were filtered through filter paper (Whatman no.1) and then dried in an oven at 70 °C until they attained a constant weight. The weights of film samples were measured in triplicate for each test. Water solubility was calculated with following equation described previously (Sadegh-Hassani & Mohammadi-Nafchi, 2014).

$$\text{Solubility (\%)} = \frac{(\text{Initial dried weight of film} - \text{Final dried weight of film})}{\text{Initial dried weight of film}} \times 100 \quad (4)$$

2.3.5. Water absorption capacity

The water absorption capacity of NAC film is defined as the rate of maximum water absorbed by the film to achieve the desired consistency. The water absorption capacity of NAC film was determined by following the procedure previously described (Sadegh-Hassani & Mohammadi-Nafchi, 2014). Briefly, NAC films (40 × 30 mm ≈ 200 mg) were firstly dried in 60 °C for 2 h and then weighed. Afterward, the dried NAC film strips were added to 150 mL of distilled water and permitted to stand for 2 h for swelling. Finally, the swollen films were weighted after draining and this procedure was performed in triplicate for each film measurement. The amount of water retained by the NAC films per dried weight sample was calculated using the following equation.

$$\text{Water absorption capacity (\%)} = \frac{(\text{Final weight after water absorptiom} - \text{Initial weight}}{\text{Initial weight}} \times 100 \quad (5)$$

2.3.6. Water vapor permeability

Water vapor permeability (WVP) is considered as a property of NAC film that permits the passage of water vapor through the microspore of NAC film. The WVP of NAC film was determined gravimetrically using a dry cup method described in the previous study with slight modification (Chaichi et al., 2017). Briefly, the test cup was filled with distilled water (15 mL) and then tightly covered with NAC film strips (diameter: 22 mm). Afterwards, each cup sample with film was initially weighed and then placed into the desiccator with ≤10% RH for 1 days. Subsequently, each cup was weighed again to evaluate the water vapor permeability of NAC film. The WVP of the film was calculated as the ratio of weight loss of water per unit square area of the film sample with the following equation.

$$\mathrm{WVP} = \frac{\text{Initial weight of cup sample} - \text{Final weight of cup sample}}{\text{Area of film used}} \quad (6)$$

2.3.7. Viscosity measurements

The viscosity of the NAC film suspension was determined by following the procedure previously described with minor modification (Chen et al., 2019). To determine the viscosity of the film suspension, rheometer (ATS Rheosystems, Bordentown, NJ, USA) was used and fixed it at room temperature (20 ± 0.1 °C). The temperature of the tested samples was monitored by platinum resistance thermometer sensors (accuracy of ± 0.1 °C) and controlled by a Peltier system. The NAC suspension of 15 mL volume was poured into a rheometer cup and then the viscometer spindle was dipped into the cup solution for 2 min to obtain thermal equilibrium conditions between spindle and the NAC suspension. Then, the rheometer spindle was operated at 30 rpm with continued shearing. Tests for each film suspension were performed in triplicate.

2.3.8. Fourier transform infrared spectroscopy

A Tensor 37 spectrophotometer was used to inspect the interactions between nanocellulose and activated carbon through the fourier transform infrared spectroscopy (FTIR) spectra. The sample holder of FTIR for the solid films was aligned at 45° to the incident beam and parallel to the ground. The range of FTIR spectra was performed with 500 to 4000 cm^{-1} and collected with 64 scans with regulation of 4.0 cm^{-1} by the omnic spectroscopy software (Dai, Zhang & Cheng, 2019).

2.3.9. Scanning electron microscopy

The microstructures of nanocellulose modified with activated carbon were visualized under scanning electron microscopy (SEM) (Hitachi-S-3400, filament-based SEM, MO, USA). For SEM observation, samples of the film were first cut (2 mm × 2 mm) and then dried at 60 °C for 24 h. To evaluate the internal structure, films were then immersed into liquid nitrogen and fixed into the support. Then, the film was coated with Au using a sputter-coater (DC-150, sputtering system, 10 nm of Au) prior to SEM observation. The surfaces of the Au-coated film sample were examined under an electric voltage of 10 kV at a working distance of 10 mm with a 1500 × magnification.

2.4. Statistical analysis

The measurements of each test of the film sample were replicated three times and the data were reported as an average ± standard deviation. Analysis of data were performed by a one way analysis of variance and the differences between the means were compared using the Duncan multiple range test with a defined significance level of $p < 0.05$.

3. Results and discussion

3.1. Physical properties of film

The NAC films and their surface morphology with varying CNF (wt. %) and AC (wt. %) contents have been shown in Fig. 1. The films were

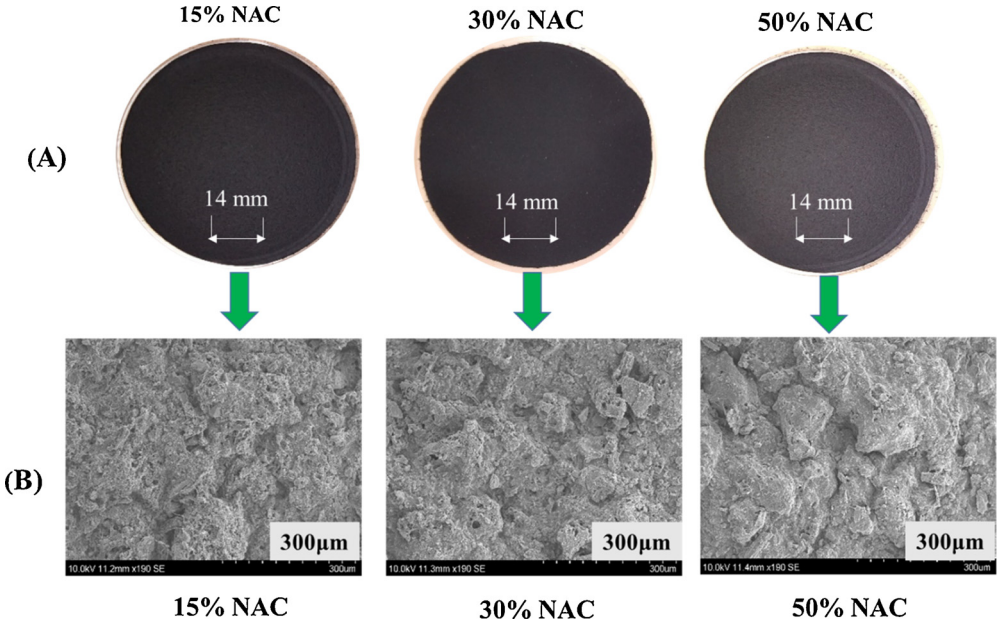

Fig. 1. Physical properties of 15%, 30% and 50% NAC films. (A) The images of NAC film with its different NAC contents (15%, 30% and 50%); (B) surface morphology of NAC films observed by scanning electron microscopy (SEM) with 300 µm.

physically and visually inspected and shown to be flexible, free standing and not transparent. The thickness and weight of each film were measured and found not significantly different from each other with increasing CNF and decreasing AC contents. The average thickness and weight (diameter: 71 mm) of films were recorded as 0.37 mm and ca. 500 mg, respectively. The produced films exhibited black color in their final appearance. But, depending on the CNF contents, an increase in the milky and opaque characteristics appeared in the film surface. These films were generally easy to handle and homogeneous with no flaws (Fig. 1A). The surface morphology of films observed under SEM indicated that 50% NAC imparted a relatively compact and hard surface compared to the 15% and 30% NAC films (Fig. 1B). Therefore, 50% NAC film formed the strongest adhesion on the interface between AC and CNF.

3.2. Electrical properties of the NAC film

The initial investigation was focused on determining the electrical properties of NAC film synthesized with varying CNF and AC contents. NAC films have AC materials that are the semiconducting ingredients; thereby they can obtain electrical conductivity. During the film formation, the hydrophilic side walls of the AC are irreversibly adsorbed onto the hydrophobic ends of CNF via π-π stacking interaction with noncovalent bonding (Wu, Wang, & Ge, 2009). Thus, the effects of CNF as a recombining agent synthesized with AC obtains resistance response during electrical analysis. Fig. 2A demonstrates that binding of CNF with AC decreased the current flow and increased the resistance (Rs) of the NAC film. As can be observed, resistance values significantly increased from 1.5 kΩ to 12.5 kΩ, when the CNF contents to the film increased from 15% to 50%. It is estimated that CNF molecules significantly increased resistance response to the film. This increase in resistances, i.e. a decrease in current, is reported by acquiring the negative charge received from non-conductive materials (Sadegh-Hassani & Mohammadi-Nafchi, 2014). Interestingly, film synthesized with $>$ 50% CNF, which means $<$ 50 AC, have not produced resistance (Rs), which confirms that NAC film blended with $\leq$ 50% CNF is suitable for producing sensor properties. Therefore, NAC films blended with $\leq$ 50 CNF and $\geq$ 50 AC can have potential for developing biosensing film for smart food packaging.

Fig. 2B shows, when the Au electrode was assembled with the 15% NAC film suspension, a significant peak current was achieved. This rise of peak current demonstrated that the suspension of 15% NAC film merged with the Au electrode employed a large surface area and enabled to efficient electron transfer in the $[Fe(CN)_6]^{3-}$ solution. After assembling the electrode with 30% NAC, the peak current decreased. When the sensing electrode surface assembled with 50% NAC, the peak current was further reduced. This current reduction indicated that the binding of CNF with the AC molecules hindered the diffusion of the redox species to the electrode surface, and thus resulted in a decrease in voltammetry current behavior. A similar current reduction was observed when non-conductive reagents (1-pyrenebutanoic acid succinimidyl ester and carboxymethyl cellulose) were immobilized on single or multi-walled carbon nanotubes (SWCNTs or MWCNTs) connected Au electrode surface (Gautam, Singh, & Yadav, 2018; Sobhan et al., 2019).

As can be seen in Fig. 2C, the 15% NAC amended electrode showed the highest peak current compared to the 30% and 50% NAC film. After increasing CNF, ranged from 30% to 50%, and decreasing AC, from 70% to 50%, the signal of peak current was further reduced. Peak current decreased with CNF content. This can be explained by the fact that decreasing AC and increasing non-conductive CNF in the film improved steric inhibition between the reducible groups; therefore they reduced current response and hybridized the Au electrode surface.

The electrochemical impedance spectroscopy (EIS) was identified using 15%, 30% and 50% NAC film deposited on the Au sensor electrode. Fig. 2D shows that the impedance of 50% NAC film was significantly higher compared to the impedance of 15% and 30% NAC. Sobhan, Oh, Park and Lee (2018) reported a similar phenomenon whereby the addition of 1-pyrenebutanoic acid succinimidyl ester to the carbon nanotube connected electrode surface caused a significant rise of impedance. Several factors could play a role in reducing the peak current and increasing the impedance. For example, one possibility is that the CNF is the nanocrystal reinforcement components and AC is the hydrophobic mesoporous components (Morán et al., 2013; Tasviri et al., 2011). After ultrasonic suspension, CNF was bonded with AC to form a dense network held together by strong inter-CNF-AC bonds, which resulted in an increase of the steric hindrance and inhibited the electrical current flow. Furthermore, increased negative charges, which was produced from the redox reaction, prevented the negatively charged $[Fe(CN)_6]^{3-}$ anions in the redox solution, and resulted in an increase in the EIS impedance (Sun et al., 2015).

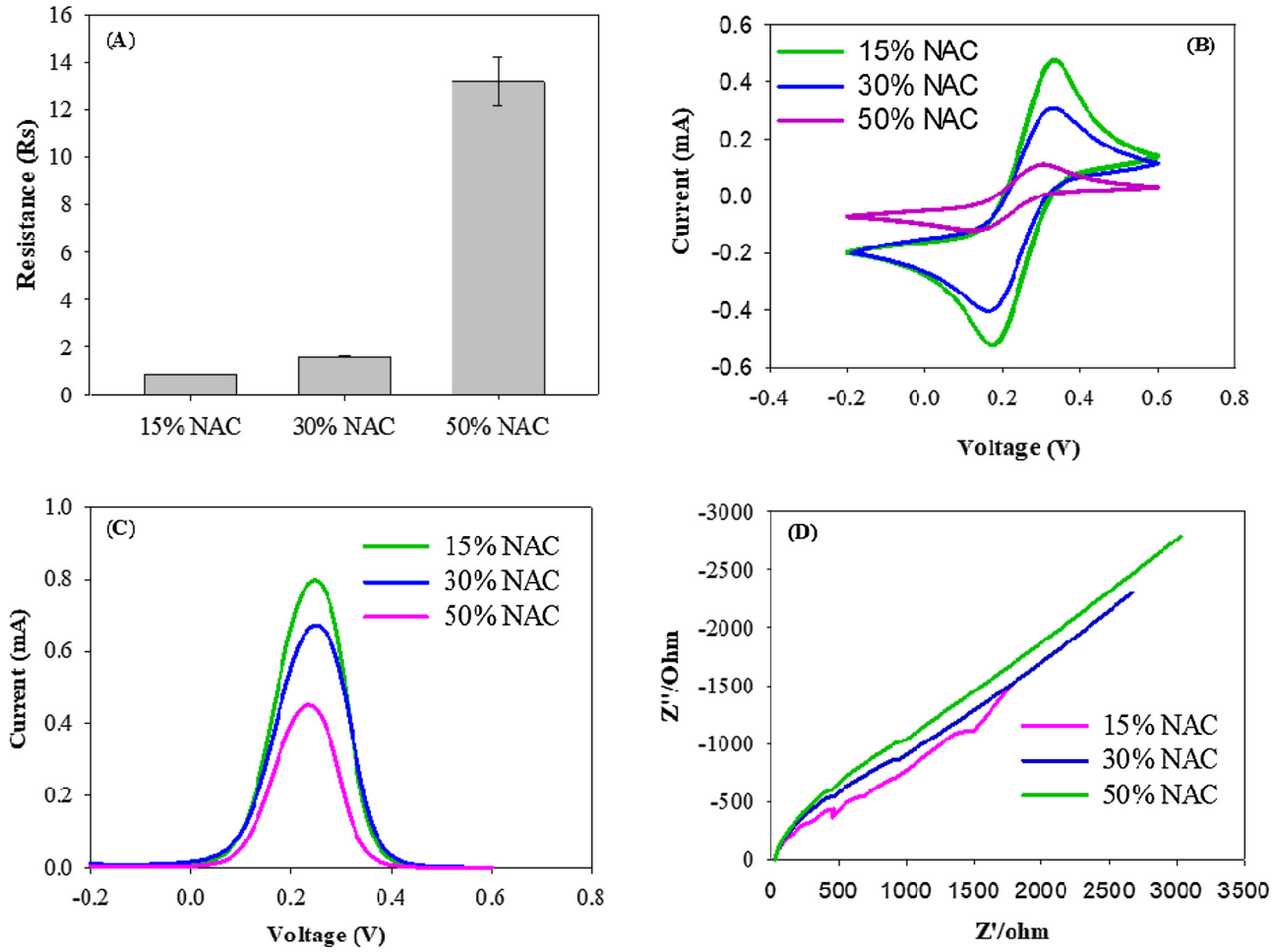

Fig. 2. Electrochemical analyses of 15%, 30% and 50% NAC films. (A) Resistance (Rs, KΩ) of NAC films measured by linear sweep voltammogram (LSV); (B) cyclic voltammogram of NAC films; and (C) differential plus voltammogram (DPV) of NAC films; (C) impedance spectra of NAC films.

3.3. Mechanical properties

As can be observed in Fig. 3, when the CNF (wt. %) increased in the film, mechanical properties, such as tensile strength (TS), strain and Young's modulus, increased simultaneously. Sadegh-Hassani and Mohammadi-Nafchi (2014) reported similar results, when biopolymer-based films combined with nanoparticles increased the TS, strain and Young's modulus. This increase of TS to packaging materials can be the vital criteria for food packaging applications (Chaichi et al., 2017); the high TS of NAC film is desired and can permit the film to resist the normal stress encountered during food shipping, handling and transportation. One possible reason of increasing TS, strain and Young's modulus is related to interfacial interaction between AC and CNF because the nanosized CNF particles, of an optimal length of 5–20 nm, are hydrophilic materials (Chen et al., 2019) which are perfectly twisted with hydrophobic particle AC and produced the rigid pathways in the

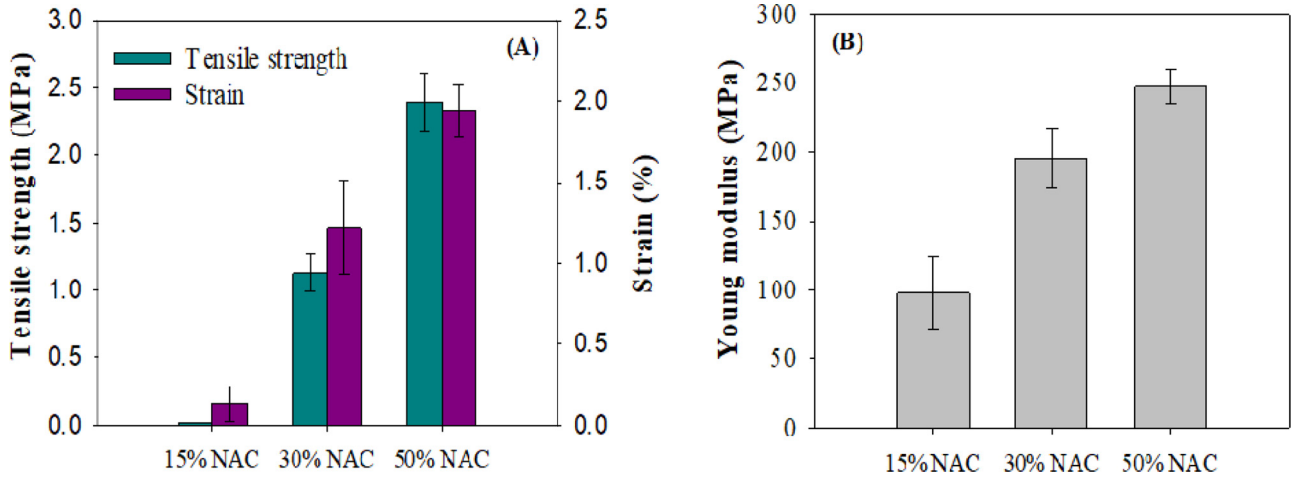

Fig. 3. Mechanical properties of 15%, 30% and 50% NAC films. (A) Tensile strength (TS) and strain of NAC films; (B) Young modulus of NAC films.

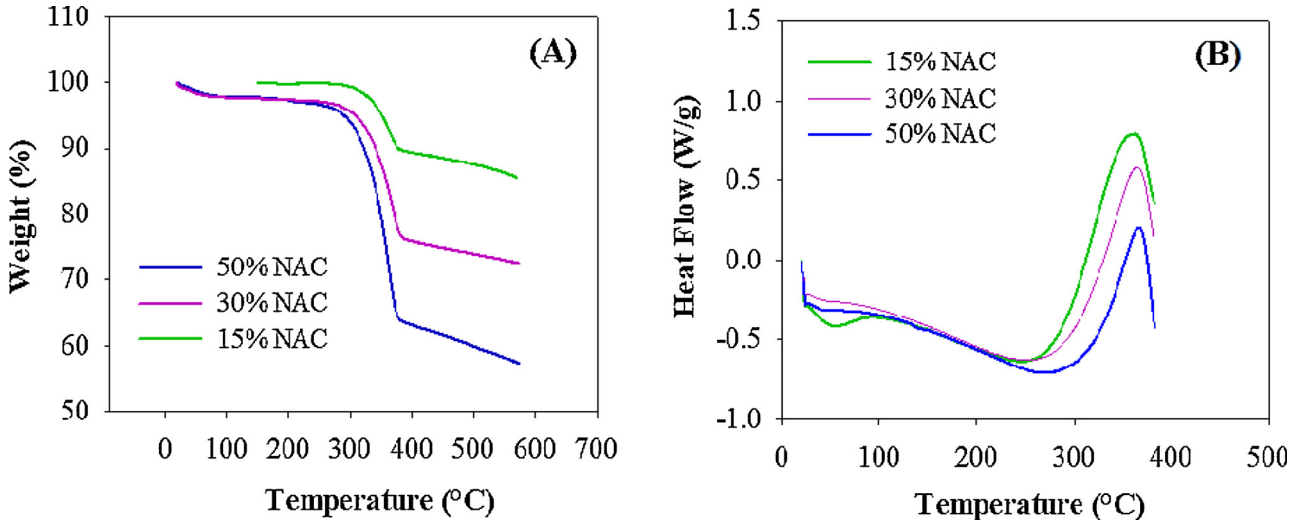

Fig. 4. Thermal analysis of 15%, 30% and 50% NAC films. (A) Typical thermogravimetric (TGA) analysis curves; (B) differential scanning calorimetry (DSC) curves of NAC film.

NAC film matrix.

The films with CNF allow more rigidity and strength during the application of tensile force, thus they resulted in a decrease in the plasticizer properties. When the 15% NAC film was employed, TS was negligible and gave under lower strain during tensile force. This illustrates that films with higher TS are more preferred and convenient for food packaging applications (Voon, Bhat, Easa, Liong, & Karim, 2012). In a previous study (Morán et al., 2013), nanoclay based polymer film produced an increased TS and Young's modulus. According to Wu et al. (2009), nanoclay particles used as a filling agent to the film increased TS and wear performance of the starch film. As 50% NAC films have significantly higher TS ($p < 0.05$) to bear the maximum applied load than the 15% and 30% NAC film, the 50% NAC film can be considered more suitable for food packaging applications.

3.4. Thermal stability of films

The thermal degradation properties of NAC films depending on the CNF and AC were determined using TGA (Fig. 4A). The degradation stages have been divided into three main regions, which occurred consecutively. In stage-I, temperature ranged between 100 to 270 °C, where physically weak and chemically strong bound water molecules were evaporated from the film sample. The second stage is the transition region, occurring between 270 and 390 °C, when NAC film composites structurally degraded and the weight losses occurred at about 60%. As can be observed, 50% NAC film was significantly degraded at this stage compared to other film contents. Therefore, it can be concluded that 15% NAC film was more rapidly crystallized than 30% and 50% NAC film sample because it has a low amount of nanocellulose than 30% and 50% NAC film. Moreover, the sample of 50% NAC film was significantly thermally affected compared to the 15% and 30% NAC film at this stage due to enhancing the thermal degradation of the large amount of nanocellulose. The third stage was seen between 390 and 590 °C. In this stage, mass loss occurred due to the carbonization of residual organic matter. The NAC film with higher CNF contents produced higher degradation, which shows that higher AC blended into the film can be thermally stable.

The thermal attributes of NAC film determined by differential scanning calorimetry (DSC) are shown in Fig. 4B. In general, the NAC sample absorbed heat and then is subjected to release of the bound water molecules until crystallization. The lowest crystallized temperature for this film appeared at ca. 280 °C. After that, NAC films began to decompose and release exothermic heat flow. The peak temperature related to melting points for NAC samples was ca. 390 °C. The heat flow rate was also considered in this study. The heat flow rate of 15% NAC film was significantly higher than those of the 30% and 50% NAC films. These results indicated that higher thermal energy was released to dissociate the interactions in the film matrix. Furthermore, 50% NAC films demonstrated lower heat flow, which may be related to the mechanism of CNF-AC interaction. This can be explained that 50% NAC films absorbed significantly higher heat and released less heat flow during the sample degradation. According to the study by Farrag et al. (2018) low heat flow is associated with strengthening the interactions in starch films treated with nanoclay. Since 15% NAC has a relatively higher percentage of AC (85%) and lower percentage of CNF (15%), it leads to significantly higher heat flow because of the enhancing of exothermic behaviors of AC in the NAC film. Therefore, it can be concluded that the thermal properties of NAC films can be affected by the method of film preparation.

3.5. Physiological properties of film

3.5.1. Water solubility and absorption capacity

The NAC films' water solubility was tested to define the comparative applications of NAC films for smart food packaging. In general, AC is highly sensitive to water molecules compared to CNF. Therefore, an increase in CNF quantity (i.e. a decrease in AC) into the film reduced water solubility performance (Fig. 5A). This is because the incorporation of CNF to the film suppresses the water diffusion rate. By incorporating the crosslinking structures or incorporation of nanoparticles to the biopolymer-based film, the water solubility rate was reduced in a similar manner (Sadegh-Hassani & Mohammadi-Nafchi, 2014). According to the Voon et al. (2012), when the nanoclay, used as a reinforcing agent, was incorporated into the starch film, the water solubility of the film decreased, which was consistent with the solubility results obtained from our test.

Water vapor permeability was also tested to verify the barrier functions of NAC film. For food packaging, a film with high vapor barrier properties is desired because it can reduce moisture transfer rates between the outside packaging environment and inside packaged food. As can be shown in Fig. 5A, 15% NAC film showed significantly higher water vapor permeability compared to 50% NAC film. As 50% NAC film is more efficient in preventing water vapor permeability than 15% and 30% NAC film, it may be preferred for food packaging application. Increasing the CNF content of the NAC film has a greatly reduced water vapor permeability (WVP). This is because CNF can fill

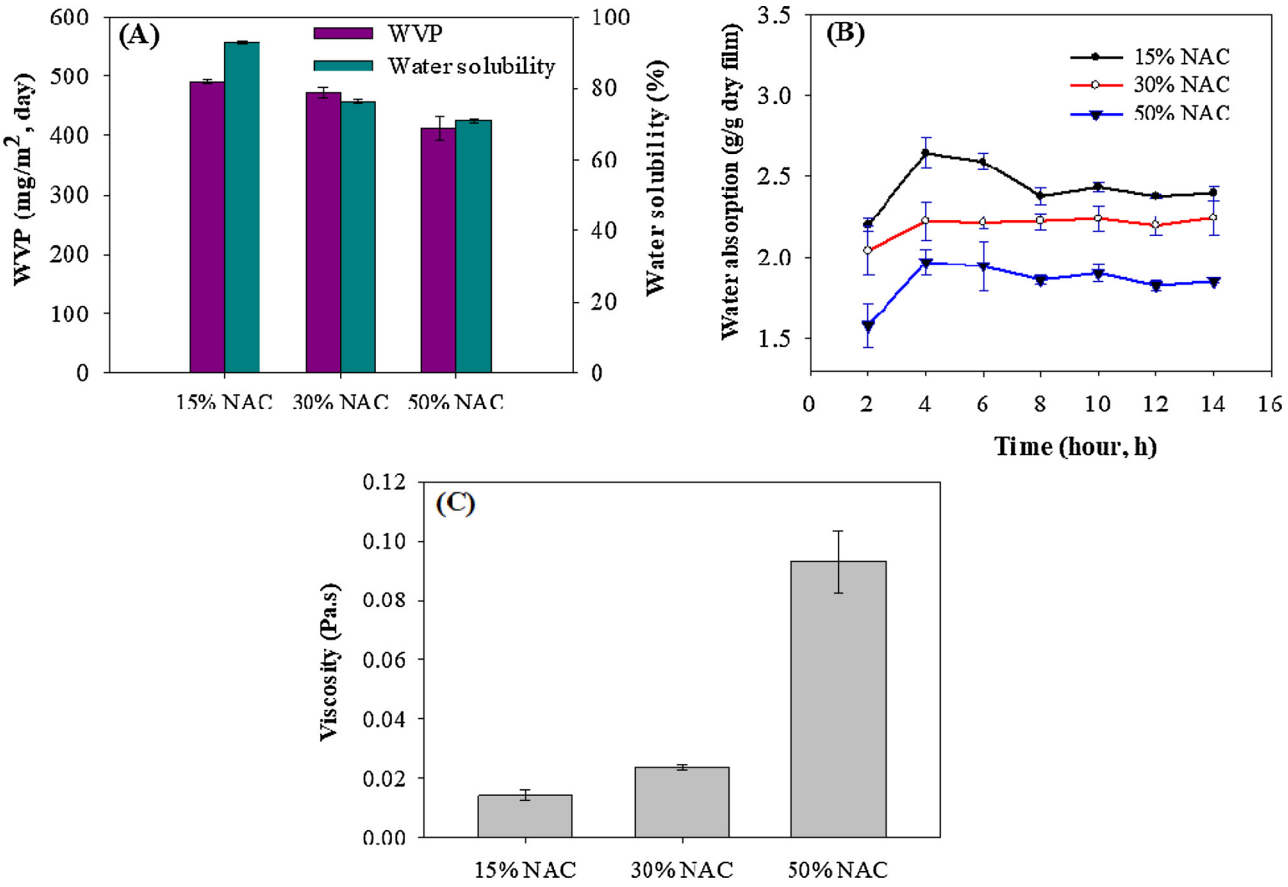

Fig. 5. Physiological properties of 15%, 30% and 50% NAC films. (A) Water vapor permeability (WVP) and water solubility of NAC film; (B) water absorption capacity of NAC film depending on time period (2, 4, 6, 8, 10, 12 h); (C) effect of nanocellulose (CNF) on the viscosity of NAC suspensions.

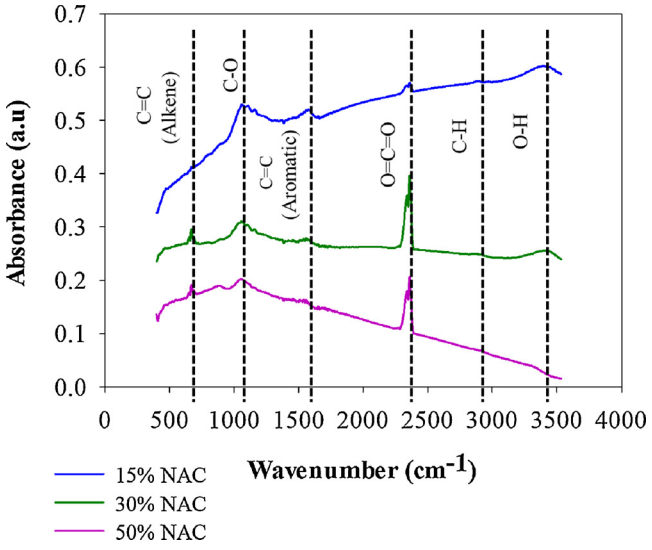

Fig. 6. Infrared spectroscopy (FTIR) spectra of 15%, 30% and 50% NAC films. The films contained different nanocellulose (CNF) and activated carbon (AC) contents.

up the microspore structures distributed over the films, thus decreasing WVP. Free water vapor molecules do not interact as strongly as with nanocomposite films alone (Chaichi et al., 2017). Chitosan-based films with added zinc oxide nanoparticles further reduced WVP significantly (Sheng et al., 2014).

Our work further determined the water absorption capacity of the NAC film; results are illustrated in Fig. 5B. As observed, the water absorption capacity of 15% NAC film was significantly higher compared to the 30% and 50% films. Conversely, water absorbance increased for all films between 2 and 4 h, then decreased from 4 to 8 h for 15% and 50% NAC film. A plateau of water absorbance capacity was observed between 2 and 14 h for 30% NAC film. Introducing an increased quantity of CNF (15% to 50%) and decreasing AC (85% to 50%) reduced the water absorption capacity. This decrease in water absorption capacity could be attributed to the hydrophobic interactions between CNF and AC in the film structure. As AC has a large surface area and porous structure, so 15% NAC film has higher absorption capacity in its microspore structure. This result was consistent with result of starch-based film (Müller, Laurindo, & Yamashita, 2011; Tunç & Duman, 2010); when the quantity of nanoclay grew in the film, water absorbance capacity decreased significantly.

Viscosity is one of the main factors that affects the processability of the casting film (Chen et al., 2019). In order to determine the effect of CNF and AC to produce NAC film, viscosity was measured using a Hybrid Rheometer. As seen in Fig. 5C, viscosity of the 50% NAC film suspension was significantly higher than 15% and 30% film suspensions. At the 15% NAC suspension, the viscosity was not affected significantly. This result was consistent with the viscosity result obtained from starch film suspension, where the quantity of laver content in the starch film increased, the viscosity of film suspension increased (Chen et al., 2019).

3.5.2. Infrared spectroscopy analysis (FTIR)

In order to ensure proper interactions between CNF and AC, FTIR spectrum was performed through UV–vis characterization and their wave spectra is presented in Fig. 6. All of the NAC films showed no significant difference in the FTIR band. The characterized peaks were displayed to 690 cm^{-1}, 1085 cm^{-1}, 1600 cm^{-1}, 2349 cm^{-1},

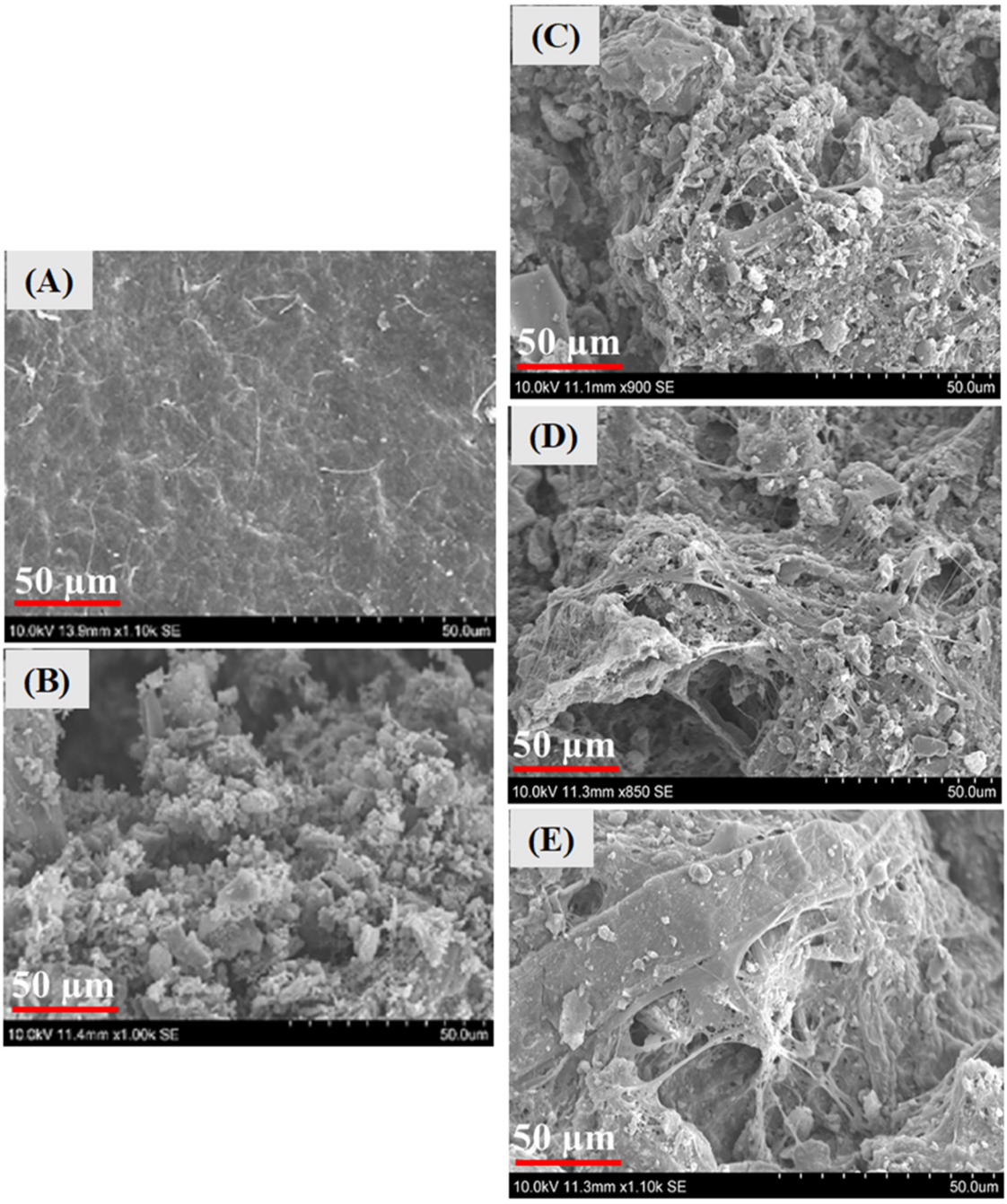

Fig. 7. SEM images of NAC film. (A) Nanocellulose (CNF); (B) activated carbon (AC); (C) 15% NAC film; (D) 30% NAC film; (E) 50% NAC film.

2900 cm^{-1} and 3450 cm^{-1}, which correlated to C═C bending (alkene), the stretching vibration of carboxy groups (C—O), aromatic carbon-carbon double bonds (C═C), carbon-dioxide bonds (O═C═O), hydrocarbon bonds (H—C) and alcohol bond (O—H, strong intermolecular bond), respectively. As observed in the Fig.6, the peak intensity associated with the NAC film decreased with increasing CNF and the intensities were dependent on the relative compositions of the NAC films. These results implied that peak intensities were influenced with the CNF concentrations and they were successfully incorporated with AC in the NAC film. Similar phenomenon was observed when peak intensities decreased as nanocellulose concentrations increased to the polyaniline based film (Liu et al., 2014).

3.5.3. SEM analysis of activated carbon

Scanning electron microscopy (SEM) is considered as an important technique for evaluating the microstructure, as well as the size distribution, of native and AC modified CNF particles. The SEM micrographs showed balanced dispersion and random direction in the NAC film. The intricate and homogenized structure indicated that two constituent elements (CNF and AC) improve the mechanical properties of NAC film. As shown in Fig. 7A, CNF formed thin fibers at the nanometer scale throughout the film and produced a compact network. The internal microscopic structures of AC with an open edge have been shown in Fig. 7B. As observed in Fig. 7C, 15% NAC film indicated an appropriate distribution of CNF nanoparticles with AC particles, which implied a suitable homogenizing method in this work. Fig. 7D showed an internal microstructure of 30% NAC film and displayed the cross-linking structure of CNF with AC materials. Fig. 7E, belonging to the 50% NAC film, illustrates abundant amounts of CNF throughout the film microstructure. White spots were observed in all the film structures

and attributed to natural impurities inside the film matrixes. It is also notable that CNF particles were well dispersed and in a more appropriate manner with AC to form the NAC film (Fig. 7E). These SEM analysis images revealed that high quantity of CNF reformed the complex film networks and interconnected structures. This result supports the decrease in water vapor permeability rates and the intricate structure suggests that the tensile properties of NAC film should increase. Dehnad, Emam-Djomeh, Mirzaei, Jafari, and Dadashi, (2014)) also explained similar microstructures of chitosan-nanocellulose biocomposites, where nanocellulose bound with chitosan particle were distributed throughout the film.

4. Conclusions

A NAC film prepared with CNF and AC was developed first time for smart food packaging applications. The study verified that the CNF contents significantly affected the physicochemical properties of NAC films. The films with higher CNF can form a compact and intricate NAC film structure. The electrical conductivity of NAC films decreased as CNF increased in the film. The increasing CNF significantly decreased the water vapor permeability and water absorption capacity but increased tensile properties of the NAC films, i.e., tensile strength (TS), strain and Young's modulus. The thermal properties of all films are thermally stable until 270 °C. The SEM images showed that the microstructural binding of CNF with AC in film structure resulted in the proper dispersion of CNF in the film. Although 50% NAC films compared to the 15% and 30% NAC films were mechanically appropriate for the rough use, they have poor electrical properties for the biosensing function which is not suitable for the smart food packaging. In addition, 30% NAC film which exhibits the good mechanical strength than 15% NAC film and has considerable electrical properties for preparing the biosensing films. Therefore, they can be considered for the food packaging. Though details of CNF and AC interaction should be investigated in future study, the properties of the NAC films show very promising potential of use in smart food packaging.

Acknowledgements

This research was funded by (1) North Central Regional Sun Grant Center at South Dakota State University through a grant provided by USDA NIFA (Grant No. SA1500640); and (2) the Hatch Project (No. 3AR652 and 3AH658) fund by USDA NIFA through South Dakota Agricultural Experimental Station at South Dakota State University.

References

Biji, K. B., Ravishankar, C. N., Mohan, C. O., & Srinivasa-Gopal, T. K. (2015). Smart packaging systems for food applications: A review. *Journal of Food Science and Technology, 52*, 6125–6135. https://doi.org/10.1007/s13197-015-1766-7.

Cao, Z., Pan, H., Chen, Y., Han, L., Bian, J., Zhang, H., et al. (2019). Ductile and biodegradable poly (lactic acid) matrix film with layered structure. *International Journal of Biological Macromolecules* (Accepted).

Chaichi, M., Hashemi, M., Badii, F., & Mohammadi, A. (2017). Preparation and characterization of a novel bionanocomposite edible film based on pectin and crystalline nanocellulose. *Carbohydrate Polymers, 157*, 167–175. https://doi.org/10.1016/j.carbpol.2016.09.062.

Chen, Y., Yu, L., Ge, X., Liu, H., Ali, A., Wang, Y., et al. (2019). Preparation and characterization of edible starch film reinforced by laver. *International Journal of Biological Macromolecules, 129*, 944–951.

Dai, L., Zhang, J., & Cheng, F. (2019). Effects of starches from different botanical sources and modification methods on physicochemical properties of starch-based edible films. *International Journal of Biological Macromolecules, 132*, 897–905.

Dehnad, D., Emam-Djomeh, Z., Mirzaei, H., Jafari, S. M., & Dadashi, S. (2014). Optimization of physical and mechanical properties for chitosan- nanocellulose biocomposites. *Carbohydrate Polymers, 105*, 222–228. https://doi.org/10.1016/j.carbpol.2014.01.094.

Farrag, Y., Malmir, S., Montero, B., Rico, M., Rodríguez-Llamazares, S., Barral, L., et al. (2018). Starch edible films loaded with donut-shaped starch microparticles. *LWT, 98*, 62–68.

Gautam, V., Singh, K. P., & Yadav, V. L. (2018). Preparation and characterization of green-nano-composite material based on polyaniline, multiwalled carbon nano tubes and carboxymethyl cellulose: For electrochemical sensor applications. *Carbohydrate Polymers, 189*, 218–228. https://doi.org/10.1016/j.carbpol.2018.02.029.

Gupta, S. M., & Tripathi, M. (2011). A review of TiO2 nanoparticles. *Chinese Science Bulletin, 56*, 1639–1657. https://doi.org/10.1007/s11434-011-4476-1.

Hayat, A., Rhouati, A., Mishra, R. K., Alonso, G. A., Nasir, M., Istamboulie, G., et al. (2016). An electrochemical sensor based on TiO2/activated carbon nanocomposite modified screen printed electrode and its performance for phenolic compounds detection in water samples. *International Journal of Environmental Analytical Chemistry, 9*, 237–246.

Jian, G., Ju, H., Hu, Z., Deng, S., & Lei, J. (2009). A glucose biosensor based on direct electrochemistry of glucose oxidase immobilized on nitrogen-doped carbon nanotubes. *Biosensors & Bioelectronics, 25*, 373–377. https://doi.org/10.1016/j.bios.2009.07.016.

Jamróz, E., Kopel, P., Juszczak, L., Kawecka, A., Bytesnikova, Z., Milosavljević, V., et al. (2018). Development and characterisation of furcellaran-gelatin films containing SeNPs and AgNPs that have antimicrobial activity. *Food Hydrocolloids, 83*, 9–16.

Jafari, A., & Amini, A. (2019). Lactic acid gas sensor based on polypyrrole thin film. *Materials Letters, 236*, 175–178.

Kim, J. H., Cho, S., Bae, T. S., & Lee, Y. S. (2014). Enzyme biosensor based on an N-doped activated carbon fiber electrode prepared by a thermal solid-state reaction. *Sensors and Actuators B, Chemical, 197*, 20–27. https://doi.org/10.1016/j.snb.2014.02.054.

Liu, C. Y., & Hu, J. M. (2009). Hydrogen peroxide biosensor based on the direct electrochemistry of myoglobin immobilized on silver nanoparticles doped carbon nanotubes film. *Biosensors & Bioelectronics, 24*, 2149–2154. https://doi.org/10.1016/j.bios.2008.11.007.

Liu, D. Y., Sui, G. X., & Bhattacharyya, D. (2014). Synthesis and characterisation of nanocellulose-based polyaniline conducting films. *Composites Science and Technology, 99*, 31–36.

Mani, V., Devadas, B., & Chen, S. M. (2013). Direct electrochemistry of glucose oxidase at electrochemically reduced graphene oxide-multiwalled carbon nanotubes hybrid material modified electrode for glucose biosensor. *Biosensors & Bioelectronics, 41*, 309–315. https://doi.org/10.1016/j.bios.2012.08.045.

Morán, J. I., Vázquez, A., & Cyras, V. P. (2013). Bio-nanocomposites based on derivatized potato starch and cellulose, preparation and characterization. *Journal of Materials Science, 48*, 7196–7203. https://doi.org/10.1007/s10853-013-7536-x.

Müller, C. M. O., Laurindo, J. B., & Yamashita, F. (2011). Effect of nanoclay incorporation method on mechanical and water vapor barrier properties of starch-based films. *Industrial Crops and Products, 33*, 605–610. https://doi.org/10.1016/j.indcrop.2010.12.021.

Mohebi, E., & Marquez, L. (2015). Intelligent packaging in meat industry: An overview of existing solutions. *Journal of Food Science and Technology, 52*, 3947–3964.

Najafi, M., Khalilzadeh, M. A., & Karimi-Maleh, H. (2014). A new strategy for determination of bisphenol A in the presence of Sudani using a ZnO/CNTs/ionic liquid paste electrode in food samples. *Food Chemistry, 158*, 125–131. https://doi.org/10.1016/j.foodchem.2014.02.082.

Niazi, M. B. K., Jahan, Z., Berg, S. S., & Gregersen, Ø. W. (2017). Mechanical, thermal and swelling properties of phosphorylated nanocellulose fibrils/PVA nanocomposite membranes. *Carbohydrate Polymers, 177*, 258–268.

Ortolani, T. S., Pereira, T. S., Assumpção, M. H. M. T., Vicentini, F. C., Gabriel de Oliveira, G., & Janegitz, B. C. (2019). Electrochemical sensing of purines guanine and adenine using single-walled carbon nanohorns and nanocellulose. *Electrochimica Acta, 298*, 893–900. https://doi.org/10.1016/j.electacta.2018.12.114.

Pacquit, A., Lau, K. T., McLaughlin, H., Frisby, J., Quilty, B., & Diamond, D. (2006). Development of a volatile amine sensor for the monitoring of fish spoilage. *Talanta, 69*, 515–520.

Qiu, J., Zhang, S., & Zhao, H. (2011). Recent applications of TiO2 nanomaterials in chemical sensing in aqueous media. *Sensors and Actuators B, Chemical, 160*, 875–890. https://doi.org/10.1016/j.snb.2011.08.077.

Remedio, L. N., dos Santos, J. W. S., Maciel, V. B. V., Yoshida, C. M. P., & de Carvalho, R. A. (2019). Characterization of active chitosan films as a vehicle of potassium sorbate or nisin antimicrobial agents. *Food Hydrocolloids, 87*, 830–838.

Sadegh-Hassani, F., & Mohammadi-Nafchi, A. (2014). Preparation and characterization of bionanocomposite films based on potato starch/halloysite nanoclay. *International Journal of Biological Macromolecules, 67*, 458–462. https://doi.org/10.1016/j.ijbiomac.2014.04.009.

Scognamiglio, V. (2013). Nanotechnology in glucose monitoring: Advances and challenges in the last 10 years. *Biosensors & Bioelectronics, 47*, 12–25.

Sevilla-Solís, M., & Fuertes-Arias, A. B. (2014). Direct synthesis of highly porous interconnected carbon nanosheets and their application as high-performance supercapacitors. *ACS Nano, 8*, 5069–5078.

Sevilla, M., Yu, L., Zhao, L., Ania, C. O., & Titiricic, M. M. (2014). Surface modification of CNTs with N-doped carbon: An effective way of enhancing their performance in supercapacitors. *ACS Sustainable Chemistry & Engineering, 2*, 1049–1055.

Sheng, M., Gao, Y., Sun, J., & Gao, F. (2014). Carbon nanodots-chitosan composite film: A platform for protein immobilization, direct electrochemistry and bioelectrocatalysis. *Biosensors & Bioelectronics, 58*, 351–358. https://doi.org/10.1016/j.bios.2014.03.005.

Sheng, Q., Luo, K., Li, L., & Zheng, J. (2009). Direct electrochemistry of glucose oxidase immobilized on NdPO4 nanoparticles/chitosan composite film on glassy carbon electrodes and its biosensing application. *Bioelectrochemistry, 74*, 246–253.

Sobhan, A., Lee, J., Park, M.-K., & Oh, J.-H. (2019). Rapid detection of Yersinia enterocolitica using a single–walled carbon nanotube-based biosensor for Kimchi product. *LWT, 108*, 48–54.

Sobhan, A., Oh, J.-H., Park, M.-K., Kim, S. W., Park, C., & Lee, J. (2018). Assessment of peanut allergen Ara h1 in processed foods using a SWCNTs-based nanobiosensor. *Bioscience, Biotechnology, and Biochemistry, 82*, 1134–1142.

Sobhan, A., Oh, J.-H., Park, M.-K., & Lee, J. (2018). Detection of peanut allergen Ara h 6 in commercially processed foods using a single-walled carbon nanotube–based biosensor. *Journal of AOAC International, 101*, 1558–1565. https://doi.org/10.5740/jaoacint.18-0041.

Sozer, N., & Kokini, J. L. (2009). Nanotechnology and its applications in the food sector. *Trends in Biotechnology, 27*, 82–89. https://doi.org/10.1016/j.tibtech.2008.10.010.

Sun, X., Jia, M., Guan, L., Ji, J., Zhang, Y., Tang, L., et al. (2015). Multilayer graphene-gold nanocomposite modified stem-loop DNA biosensor for peanut allergen-Ara h1 detection. *Food Chemistry, 172*, 335–342. https://doi.org/10.1016/j.foodchem.2014.09.042.

Tasviri, M., Rafiee-Pour, H. A., Ghourchian, H., & Gholami, M. R. (2011). Amine functionalized TiO2 coated on carbon nanotube as a nanomaterial for direct electrochemistry of glucose oxidase and glucose biosensing. *Journal of Molecular Catalysis B, Enzymatic, 68*, 206–210. https://doi.org/10.1016/j.molcatb.2010.11.005.

Tunç, S., & Duman, O. (2010). Preparation and characterization of biodegradable methyl cellulose/montmorillonite nanocomposite films. *Applied Clay Science, 48*, 414–424. https://doi.org/10.1016/j.clay.2010.01.016.

Veerakumar, P., Madhu, R., Chen, S. M., Hung, C. T., Tang, P. H., Wang, C. B., et al. (2014). Porous carbon-modified electrodes as highly selective and sensitive sensors for detection of dopamine. *Analyst, 139*, 4994–5000.

Vigneshwaran, N., Mhaske, S. T., Savadekar, N. R., Karande, V. S., & Bharimalla, A. K. (2012). Preparation of nano cellulose fibers and its application in kappa-carrageenan based film. *International Journal of Biological Macromolecules, 51*, 1008–1013.

Voon, H. C., Bhat, R., Easa, A. M., Liong, M. T., & Karim, A. A. (2012). Effect of addition of halloysite nanoclay and SiO_2 nanoparticles on barrier and mechanical properties of bovine gelatin films. *Food and Bioprocess Technology, 5*, 1766–1774.

Wu, M., Wang, M., & Ge, M. (2009). Investigation into the performance and mechanism of SiO_2 nanoparticles and starch composite films. *Journal of the Textile Institute, 100*, 254–259. https://doi.org/10.1080/00405000701757677.